Video Article

In Vivo Imaging of *Cx3cr1*$^{gfp/gfp}$ Reporter Mice with Spectral-domain Optical Coherence Tomography and Scanning Laser Ophthalmoscopy

Despina Kokona[1], Joël Jovanovic[1], Andreas Ebneter[1], Martin S. Zinkernagel[1]

[1]Department of Ophthalmology and Department of Clinical Research, Bern University Hospital and University of Bern

Correspondence to: Despina Kokona at Despina.Kokona@insel.ch

URL: https://www.jove.com/video/55984
DOI: doi:10.3791/55984

Keywords: Medicine, Issue 129, Microglia, retina, optical coherence tomography, scanning laser ophthalmoscopy, *in vivo* imaging, ophthalmology

Date Published: 11/11/2017

Citation: Kokona, D., Jovanovic, J., Ebneter, A., Zinkernagel, M.S. *In Vivo* Imaging of *Cx3cr1*$^{gfp/gfp}$ Reporter Mice with Spectral-domain Optical Coherence Tomography and Scanning Laser Ophthalmoscopy. *J. Vis. Exp.* (129), e55984, doi:10.3791/55984 (2017).

Abstract

Spectral domain optical coherence tomography (SD-OCT) and scanning laser ophthalmoscopy (SLO) are extensively used in experimental ophthalmology. In the present protocol, mice expressing green fluorescent protein (gfp) under the promoter of *Cx3cr1* (BALB/c-*Cx3cr1*$^{gfp/gfp}$) were used to image microglia cells *in vivo* in the retina. Microglia are resident macrophages of the retina and have been implicated in several retinal diseases[1,2,3,4,5,6]. This protocol provides a detailed approach for generation of retinal B-scans, with SD-OCT, and imaging of microglia cell distribution in *Cx3cr1*$^{gfp/gfp}$ mice with SLO *in vivo*, using an ophthalmic imaging platform system. The protocol can be used in several reporter mouse lines. However, there are some limitations to the protocol presented here. First, both SLO and SD-OCT, when used in the high-resolution mode, collect data with high axial resolution but the lateral resolution is lower (3.5 µm and 6 µm, respectively). Moreover, the focus and saturation level in SLO is highly dependent on parameter selection and correct alignment of the eye. Additionally, using devices designed for human patients in mice is challenging due to the higher total optical power of the mouse eye compared to the human eye; this can lead to lateral magnification inaccuracies[7], which are also dependent on the magnification by the mouse lens among others. However, despite that the axial scan position is dependent upon lateral magnification, the axial SD-OCT measurements are accurate[8].

Video Link

The video component of this article can be found at https://www.jove.com/video/55984/

Introduction

In experimental ophthalmology, examination of retinal pathology is usually evaluated using histological techniques. However, histology requires animal euthanization and may cause alteration to the actual properties of the tissue. SD-OCT and SLO are routinely used in clinical ophthalmology for diagnostic purposes and for the monitoring of several retinal diseases such as diabetic macular edema[9], anterior ischemic optic neuropathy[10], or retinitis pigmentosa[11]. SD-OCT and SLO are non-invasive techniques that generate high-resolution images of the retina, which are visualized through the dilated pupil without further intervention. SD-OCT provides information of retinal structure and retinal thickness by collecting backscattering data to create cross-sectional images of the retina, while SLO collects fluorescence data to produce stereoscopic high-contrast images of the retina. Nowadays, both techniques are increasingly used in experimental ophthalmology using small rodents[12,13,14,15] (or even zebrafish[16,17]) and can provide both qualitative and quantitative information[12,17,18,19,20,21].

Accumulation of endogenous fluorophores like lipofuscins or the formation of drusen in the retina can be visualized by SLO as auto fluorescent signal. This feature makes SLO a valuable technique for diagnosis and monitoring of retinal diseases such as age-related macular degeneration or retinitis pigmentosa[22,23]. In experimental ophthalmology, auto fluorescence imaging (AF) can be used for the detection of specific cell types in reporter mouse lines. For example, mice heterozygous for the expression of gfp under the promoter of *Cx3cr1*[24] are advantageous for *in vivo* visualization of microglial cells in the normal retina and for the investigation of microglia/macrophage dynamics in retinal disease[21]. Microglia are the resident macrophages of the retina, which play a crucial role on tissue homeostasis and tissue repair upon injury[1,25,26]. Microglia activation in the retina has been reported in retinal injury, ischemia, and degeneration, suggesting a role of these cells in retinal disease[2,3,4,5,6].

The aim of the present protocol is to describe a relatively simple method for retinal imaging and measurement of retinal thickness using SD-OCT, and for visualization of gfp positive microglia cells in the *Cx3cr1*$^{gfp/gfp}$ mouse retina using SLO (Heidelberg Spectralis HRA+OCT system). This protocol can be utilized for imaging and thickness measurements of healthy or diseased retinas in various mouse lines. Additionally, morphometric analyses can be performed for the identification and quantification of microglia numbers and microglia activation in the retina using SLO[21]. Microglia cells are associated with degenerative diseases in the central nervous system (CNS), including the retina[27,28,29]. Thus, by combining the two methods used in the present protocol, correlation of microglia distribution and retinal degeneration can be made, which can facilitate monitoring disease severity or the effectiveness of therapeutic approaches *in vivo*.

Protocol

In all procedures, BALB/c adult male and female mice who express gfp under the promoter of *Cx3cr1* were used[24]. Mice were treated according to the ARVO Statement for the Use of Animals in Ophthalmic and Vision Research and all procedures were approved from the Swiss government according to the Federal Swiss Regulations on Animal Welfare. Mice were anesthetized by a subcutaneous injection of medetomidine hydrochloride (0.75 mg/kg) and ketamine (45 mg/kg). Proper anesthesia was confirmed by monitoring the respiratory rate and the animal's reflex against a tail pinch. At the end of the experiments, mice were euthanized with CO_2 inhalation.

NOTE: Perform each imaging session as quickly as possible (maximum 20 min), since cataract formation following anesthesia may hamper retinal visualization[30].

1. System Configuration

1. Turn on the computer.
2. Turn on the power supply. The message "Start acquisition module" will appear on the device`s control panel screen.
3. Double click on the software`s desktop shortcut to operate the software.
4. On the database view, click the "add patient" icon.
5. In the pop-up window, insert all necessary information (last name, first name, title, date of birth, sex, and patient-ID) and click "ok". On the pop window set the corneal curvature to 2 mm and click "ok".
6. Position a 78D standard ophthalmic non-contact slit lamp lens in front of the standard 30 ° optic and fasten it safely with tape.
7. Make sure that the filter lever on the left of the device is positioned on the indication "A" to allow both IR+OCT and AF imaging (**Figure 1**).

2. Mouse Preparation

1. Use a medetomidine hydrochloride dose of 0.75 mg/kg and a ketamine dose of 45 mg/kg in phosphate-buffered saline (PBS, pH 7.4) to prepare anesthesia solution. Thus, for a 20 g mouse, mix 15 µL of medetomidine hydrochloride with 18 µL of ketamine to a final volume of 50 µL in PBS. Store the solution at 4 °C for up to one week.
2. Grasp the mouse by the scruff and apply one drop of tropicamide 0.5% + phenylephrine hydrochloride 2.5% on each eye to achieve pupil dilation.
3. Keep the mouse restrained, and with an insulin syringe attached to a 30G needle, inject 50 µL of the anesthesia solution subcutaneously. Put the mouse back in its cage that is placed above a heating pad. Wait 3-5 min until the mouse is fully sedated. To assess anesthetic depth, pinch the tail of the mouse. Check the corneal reflex by gently touching the mouse cornea with a cotton swab. If no positive reflex is observed, continue with the imaging.
   NOTE: It is important to monitor respiratory rate during anesthesia. If the mouse is not fully sedated, the respiratory rate will increase upon a painful stimulus.
4. Hydrate the mouse cornea with an application of 2% hydroxypropylmethylcellulose drops on each eye.

3. SD-OCT

1. Place a warming patch of approximately 32 °C on the custom-made platform attached on the device`s chin rest (**Figure 1**).
2. To image the right eye, place the mouse on the left part of the platform (**Figure 1**). Ensure that the right orbit of the mouse faces the lens and its body lies prone on the left part of the platform.
3. Apply a drop of hydroxypropylmethylcellulose on the right eye and carefully position a +4 diopter rigid gas permeable contact lens on it (spherical power: -25.00 to +25.00 diopters). Store the contact lens in balanced salt solution (BSS). To grab the lens, use plastic or silicon forceps to avoid damage.
4. Press the yellow box on the right corner of the control panel display to start the acquisition module (green box on **Figure 2A**). The yellow box will turn green and the control panel menu will appear on the screen (**Figure 2A**).
5. For acquisition of B-scans, select the option IR+OCT on the control panel (**Figure 2A**). Selected settings are highlighted in blue on the control panel.
6. Select "Retina" under "Application and Structure" in the software and move the lens towards the mouse eye using the micromanipulator on the device (**Figure 1**). Before focusing onto the retina, check that the indication "OD" is selected on the left bottom part of the screen. The software automatically identifies the left (OS) and the right (OD) eye based on the position of the objective.
   NOTE: If the objective is positioned on the middle of the platform, an error message will appear on the bottom of the screen. In that case, re-position the mouse slightly until the software recognizes the correct eye.
7. With the focus knob, focus on the retina until the big vessels are clearly seen in the fundus image on the left of the computer screen. Move the camera by turning the micromanipulator left or right, to move the camera in that direction, or clockwise or counterclockwise, to move the camera up or down, respectively.
   NOTE: Reposition the mouse on the platform or move the lens upwards or downwards to achieve the preferred localization of the optic nerve head in the infrared image.
8. Turn the sensitivity knob counterclockwise to reduce or clockwise to increase the brightness of the fundus image. When optimal focus is achieved, an SD-OCT B-scan will appear on the right of the screen.
   NOTE: If the B-scan cannot be visualized by adjusting the focus, press the combination Ctrl+Alt+Shift+O on the keyboard. In the pop-up window, adjust the value of the reference arm until the B-scan appears on the screen.
9. On the bottom right of the screen, choose the single scan from the pattern menu (single line in **Figure 2B**).
10. Turn the micromanipulator of the device (**Figure 1**) left, right, forward, or backward (to turn the camera in that direction) to ensure that the B-scan is located between the top and bottom corners of the SD-OCT scan window.

11. Set the Automatic Real-Time (ART) value to at least 9 to obtain high quality images.
    NOTE: ART improves image quality by averaging several consecutive scans. The higher the "ART" value, the higher the signal-to-noise ratio and thus the image quality. However, by increasing the "ART" value, the acquiring time is also increased.
12. Press the "acquire" button (**Figure 2**) on the control panel screen and acquire the images.
13. Re-position the mouse to image the left eye and repeat steps 3.2-3.12.
14. Remove the contact lens with plastic/silicon forceps and place it into BSS.
15. Hydrate the mouse cornea with a fresh drop of hydroxypropylmethylcellulose and remove the excess with a tissue paper.
16. Remove the standard 30 ° optic by rotating it counterclockwise.
17. Mount the 55 ° lens and repeat steps 3.4-3.12 for each eye.

4. Auto Fluorescence Imaging

1. Without moving the mouse on the platform, select IR on the control panel.
2. With the focus knob, focus on the big retinal vessels.
3. On the control panel select AF.
4. Turn the sensitivity knob counterclockwise to reduce or clockwise to increase the brightness of the image.
5. Press the sensitivity knob and set the "ART" value to 67 or more to obtain high quality images.
6. When the set "ART" value has been reached, press "acquire" on the control panel to acquire the image. Press the sensitivity knob again to stop averaging. Adjust the focus, to visualize different retinal layers.
7. Remove the 55° lens and mount the wide field 102° lens. Follow steps 4.1–4.6 for both eyes of each mouse and for every mouse.
8. Click “Save images” on the left upper border of the window and then click “exit”. To save the images in the computer, select the mouse from the list on the right part of the screen by double clicking on the mouse name. Double click on each image separately and then click on the floppy disc icon. Save the image as .tif, .bmp, .jpg, or .png at the desired folder. To exit the software press “File” and “Exit”.

5. Anesthesia Reversal

1. Hydrate the mouse eyes with one drop of hydroxypropylmethylcellulose and return the mouse on a heating pad.
2. Prepare atipamezole solution in a dose of 2.25 mg/kg to reverse the sedative effects of medetomidine hydrochloride. For a 20 g mouse, add 9 µL of atipamezol in a final volume of 150 µL PBS. Store the solution at 4 °C for up to one week.
3. min after anesthesia injection (step 2.2), inject 150 µL of atipamezole solution subcutaneously.
4. Monitor the mouse until recovery from anesthesia. When the mouse is fully recovered (5-10 min after atipamezole injection) put it back in its cage. Recovery is indicated by the ability of the animal to turn its body when laid on one side, regaining of walking activity, and reacting in response to environmental stimulation.

6. Manual Retinal Thickness Measurement from SD-OCT Images

1. Open the OCT scan by double clicking on the name of the animal.
2. Open the B-scan obtained with the 30 ° or 55 ° lens.
3. Choose "thickness profile".
4. Press the "Edit Layer Segmentations" icon (**Figure 2B**). The software automatically identifies the inner limiting and base membrane.
5. If necessary, manually correct the position of the inner limiting and base membrane. To do so, choose the layer to be modified from the left side of the screen and then the red circle option (**Figure 2B**). Move the circle with the mouse button pressed to modify the line.
6. Modify the line to position the corresponding layer correctly. Click "Save and close" to exit the window.
   NOTE: Due to reflectivity of the choroid, the software may identify the base membrane incorrectly. Thus, it is preferable to define it manually before proceeding to retinal thickness measurements.
7. Choose "Retina" under the "Layer" option. A diagram of retinal thickness will appear on the bottom of the screen.
8. Click on a different position either on the diagram or on the B-scan to view the retinal thickness (indicated in µm) for the selected position.
9. Measure the retinal thickness in the desired distance from the optic nerve head and copy the values in a spreadsheet.
10. Repeat steps 5.1-5.9 for each mouse for both the 30 ° and the 55 ° lens.
11. Perform statistical analysis with desired software.

Representative Results

Using the protocol presented here, SD-OCT scans and SLO images were obtained from *Cx3cr1*$^{gfp/gfp}$ mice in the same imaging session. **Figure 3** includes representative SD-OCT single scans obtained with a 30 ° or a 55 ° lens (**Figure 3A**) and representative SLO images obtained with a 55 ° or a 102 ° lens, where gfp positive microglia cells are visualized. Higher reflectivity of the choroid is observed in the SD-OCT scans obtained with the 30 ° compared to the 55 ° lens. However, retinal architecture is clear in both the 30 ° and the 55 ° images (**Figure 3**, right magnified images). After manual corrections of retinal boundaries (inner limiting and base membrane), a good correlation of retinal thickness measurements was observed between the 30 ° and the 55 ° lens when measuring in the same distance from the optic nerve head (**Figure 3C**; Pearson correlation = 0.967, $p < 0.0001$). Previous studies have shown that retinal thickness measurements on SD-OCT scans correlate well with *ex vivo* measurements on histological retinal sections[15,31] and thus SD-OCT can be used as a non-invasive technique for retinal thickness measurements. Using SLO, we could identify gfp positive microglia cells as hyperreflective signal in the auto fluorescent images, however the wide field 102 ° lens was able to cover a larger fundus area compared to the 55 ° lens. SLO can also be utilized for the monitoring of retinal microglia cells distribution and activation in reporter mice with a functional fractalkine receptor (*Cx3cr1*$^{gfp/+}$ mice) in normal or diseased retina[12,21,32]. The combination of SD-OCT with SLO in the same imaging session can provide information about microglia distribution and activation upon retinal degeneration and could be useful for monitoring retinal diseases in mice[21].

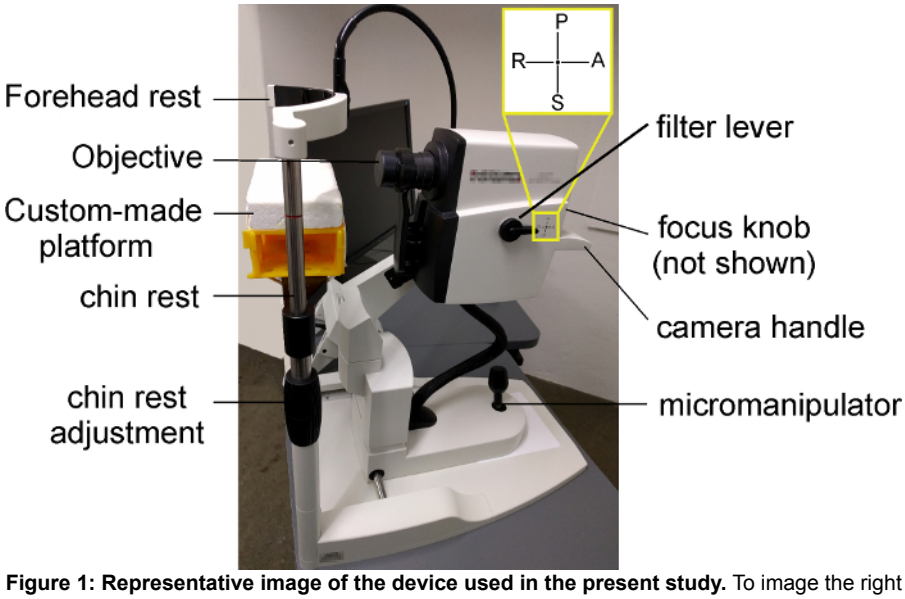

Figure 1: Representative image of the device used in the present study. To image the right eye of the mouse, the mouse is positioned on the left part of the custom-made platform with its right orbit facing the lens and its body lying prone on the left part of the platform. The height of the platform can be adjusted by turning clockwise (to lower the platform) or counterclockwise (to lift the platform up) the "chin rest adjustment". The filter lever must be positioned to "A" to allow IR+OCT and AF imaging. With the focus knob (not visible on the figure), the experimenter can change the focus of the scanner. The micromanipulator can be used to correctly illuminate and align the retina for high quality images. The objective can be moved up, down, right, or left by the camera handle. Please click here to view a larger version of this figure.

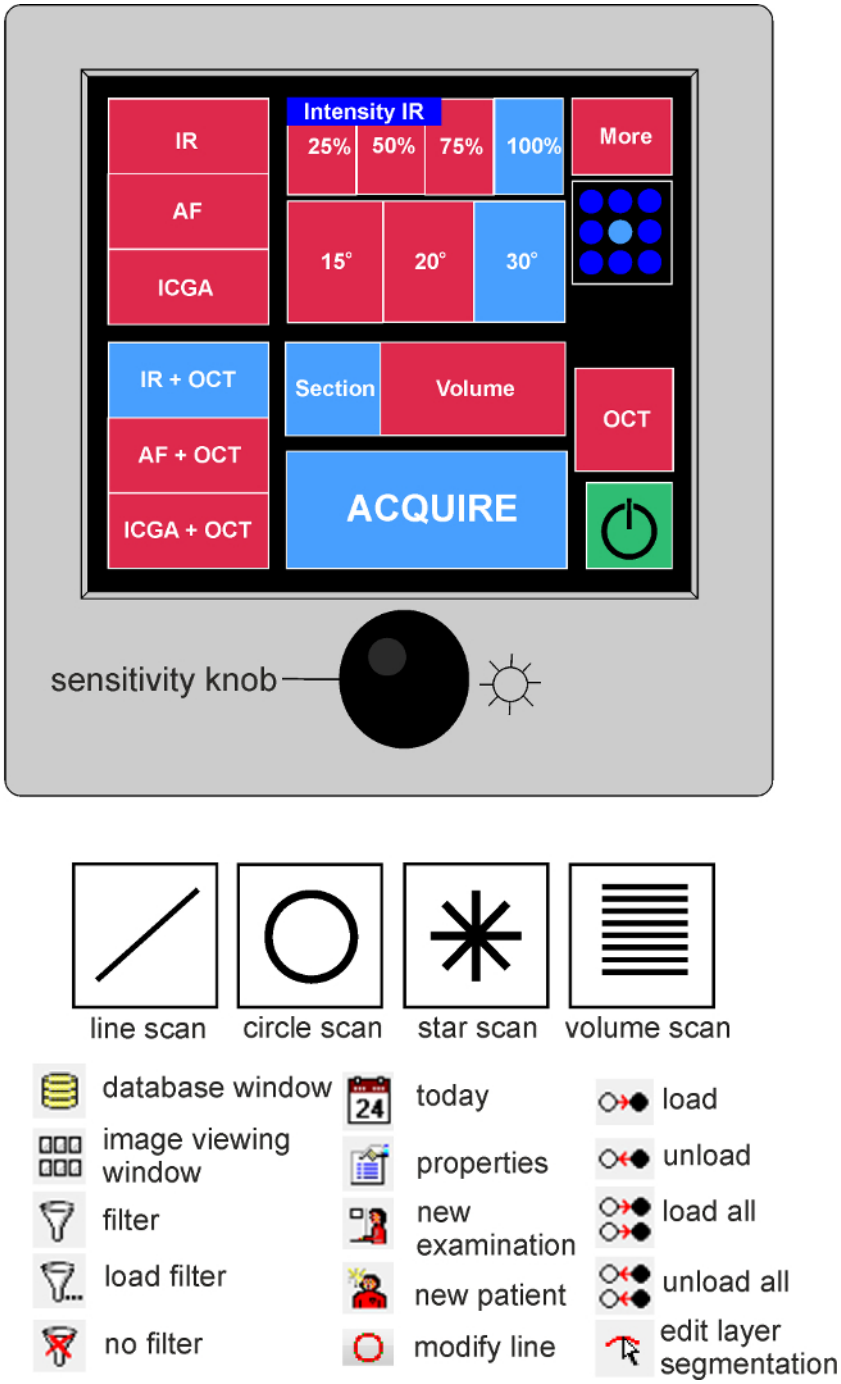

Figure 2: Illustration of the device`s control panel. (**A**) On the left part of the control panel display the acquisition modes can be selected (infrared, IR; auto fluorescence, AF or indocyanine green angiography, ICGA; combined or not with optical coherence tomography, OCT). On the middle part of the panel the acquisition setting can be chosen (intensity of the IF image, section or volume scans). The field of view is determined by the loaded lens. With the sensitivity knob the brightness of the IR or AF image can be adjusted. By pressing the sensitivity knob, the software will start averaging the images obtained in IR or AF to provide a high-quality image. (**B**) Illustration of the acquisition pattern menu. (**C**) Summary of functions used in the software with the corresponding icon. Please click here to view a larger version of this figure.

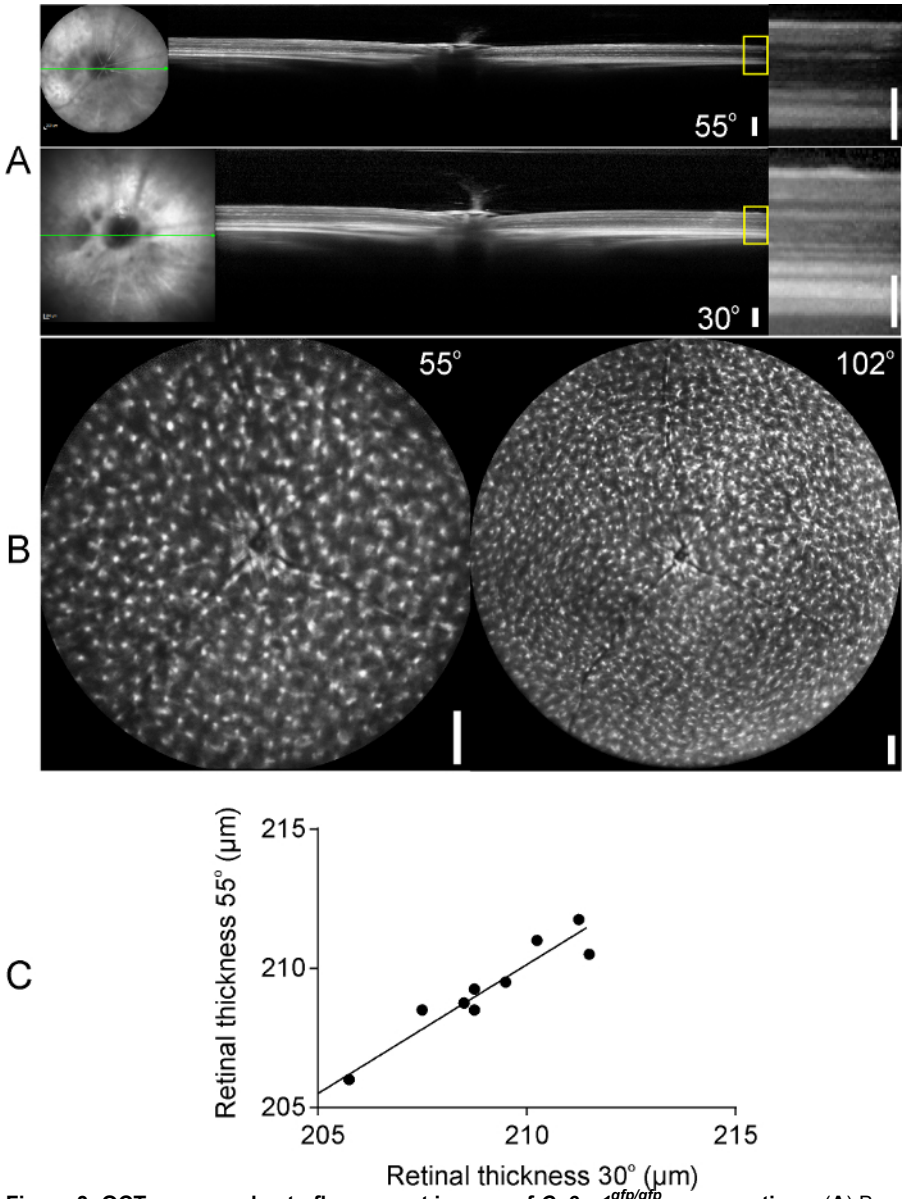

Figure 3: OCT scans and auto fluorescent images of *Cx3cr1*$^{gfp/gfp}$ mouse retinas. (**A**) B-scans of the mouse retina obtained with a 55 ° (upper panel) or a 30 ° lens (bottom panel). Higher magnifications of the yellow boxes are presented on the right panel. (**B**) Images of gfp positive microglia cells in the retinas of *Cx3cr1*$^{gfp/gfp}$ mice obtained with a 55 ° and a 102 ° lens (left and right panels, respectively). (**C**) Retinal thickness measurements, measured on the same distance from the optic nerve head, on SD-OCT scans derived from the 30 ° and 55 ° lens. A good correlation was observed between the two lenses (Pearson correlation = 0.967). Scale bars: 200 µm, 100 µm on magnified SD-OCT images (A, right panel). Please click here to view a larger version of this figure.

Discussion

The present article demonstrates a protocol for the acquisition of retinal B-scans and imaging of gfp positive microglia distribution in the mouse retina in the same imaging session. SD-OCT and SLO are increasingly used in animal models of retinal disease to provide information of retinal alterations over time[10,14,17,18,21]. With this protocol, *Cx3cr1*$^{gfp/gfp}$ or *Cx3cr1*$^{gfp/+}$ mouse retina can be non-invasively imaged and information of retinal thickness can be obtained. This is critically important in retinal disease experimental models, where disease severity changes over time or when therapeutic treatments are tested. Moreover, the protocol describes how reporter mouse lines can be utilized for the *in vivo* imaging of fluorescent cells in the retina.

However, the protocol presented here has some limitations. First, imaging of the mouse retina in devices designed for humans may be challenging due to the higher total optical power of the mouse eye, which can lead to lateral magnification inaccuracies[7]. However, the axial SD-OCT measurements are accurate[8]. Additionally, follow-up examination in mice using the "set reference" option of the software is rather difficult due to the not fixed position of the mouse on the platform and thus longitudinal imaging of mouse retinas can be challenging. Longitudinal alignment of the eye can be achieved by positioning the optic nerve in the center of the infrared image and then acquiring the desired images. In order to correct for eye rotation, manual alignments of the SD-OCT en face images can be performed after acquisition and apply to the thickness

measurements as described elsewhere[33]. Besides the imaging system used in the present protocol, other imaging systems have also been developed that provide a greater angle and can image a larger retinal area without the use of the contact lens. Optos for example can cover a larger retinal surface but with greater image variability compared to the device used in the present study[34]. Despite these limitations, the present protocol can be utilized in several experimental models of retinal disease. The information that can be obtained includes retinal thickness alterations (swelling, atrophy), detection of retinal detachment, or the presence of hyperreflective dots and fluorophore-labeled cells and the increase or decrease of their numbers.

Combination of the two methods in mice heterozygous for the expression of *Cx3cr1* (*Cx3cr1*$^{gfp/+}$), which have a functional fractalkine receptor, enables the experimenter to simultaneously detect *in vivo* alterations of retinal integrity in real time and possible microglia accumulation in the vicinity of retinal abnormalities (*e.g.*, retinal swelling, retinal atrophy) during retinal disease or injury. Moreover, by applying morphometric analysis, microglia activation state can be assessed based on the soma size and complexity of microglia processes[21]. In retinal diseases, such as retinal vein occlusion, activation and accumulation of microglia/macrophages on retinal atrophic sites have been observed[27]. Moreover, in mice defective for the *Nr2e3* gene (Nuclear Receptor Subfamily 2 Group E Member 3), a mouse model of the recessively inherited enhanced S-cone sensitivity syndrome (ESCS), the outer nuclear layer folding (rosettes) can be observed at early postnatal days.

Interestingly, microglia cells can be found inside the rosettes and it has been suggested that microglia might contribute to the degeneration of photoreceptors observed in the retinas of these mice[35,36]. Since activation of microglia have been implicated in the course of a variety of retinal diseases and sometimes is accompanied by alterations in retinal architecture[10,27,37,38], the combination of SD-OCT and SLO can reveal correlations between microglia activation and retinal degeneration. Despite some challenges, the present protocol can provide such information longitudinally, and thus it would be valuable for the correlation of retinal damage with microglia distribution/activation and for the monitoring of therapeutic treatment effectiveness[21].

Disclosures

The authors have nothing to disclose.

Acknowledgements

This work was supported by a grant of the Swiss National Science Foundation (SNSF; #320030_156019). The authors received nonfinancial support from Heidelberg Engineering GmBH, Germany.

References

1. Madeira, M. H., Boia, R., Santos, P. F., Ambrosio, A. F., & Santiago, A. R. Contribution of microglia-mediated neuroinflammation to retinal degenerative diseases. *Mediators Inflamm.* **2015** 673090 (2015).
2. Ng, T. F., & Streilein, J. W. Light-induced migration of retinal microglia into the subretinal space. *Invest Ophthalmol Vis Sci.* **42** (13), 3301-3310 (2001).
3. Langmann, T. Microglia activation in retinal degeneration. *J Leukoc Biol.* **81** (6), 1345-1351 (2007).
4. Joly, S. *et al.* Cooperative phagocytes: resident microglia and bone marrow immigrants remove dead photoreceptors in retinal lesions. *Am J Pathol.* **174** (6), 2310-2323 (2009).
5. Arroba, A. I., Alvarez-Lindo, N., van Rooijen, N., & de la Rosa, E. J. Microglia-mediated IGF-I neuroprotection in the rd10 mouse model of retinitis pigmentosa. *Invest Ophthalmol Vis Sci.* **52** (12), 9124-9130 (2011).
6. Zhang, C., Lam, T. T., & Tso, M. O. Heterogeneous populations of microglia/macrophages in the retina and their activation after retinal ischemia and reperfusion injury. *Exp Eye Res.* **81** (6), 700-709 (2005).
7. Geng, Y. *et al.* Optical properties of the mouse eye. *Biomed Opt Express.* **2** (4), 717-738 (2011).
8. Lozano, D. C., & Twa, M. D. Development of a rat schematic eye from in vivo biometry and the correction of lateral magnification in SD-OCT imaging. *Invest Ophthalmol Vis Sci.* **54** (9), 6446-6455 (2013).
9. Vaz-Pereira, S. *et al.* Optical Coherence Tomography Features Of Active And Inactive Retinal Neovascularization In Proliferative Diabetic Retinopathy. *Retina.* **36** (6), 1132-1142 (2016).
10. Kokona, D., Haner, N. U., Ebneter, A., & Zinkernagel, M. S. Imaging of macrophage dynamics with optical coherence tomography in anterior ischemic optic neuropathy. *Exp Eye Res.* (2016).
11. Makiyama, Y. *et al.* Macular cone abnormalities in retinitis pigmentosa with preserved central vision using adaptive optics scanning laser ophthalmoscopy. *PLoS One.* **8** (11), e79447 (2013).
12. Paques, M. *et al.* High resolution fundus imaging by confocal scanning laser ophthalmoscopy in the mouse. *Vision Res.* **46** (8-9), 1336-1345 (2006).
13. Joshi, R. *et al.* Spontaneously occurring fundus findings observed using confocal scanning laser ophthalmoscopy in wild type Sprague Dawley rats. *Regul Toxicol Pharmacol.* **77** 160-166 (2016).
14. Muraoka, Y. *et al.* Real-time imaging of rabbit retina with retinal degeneration by using spectral-domain optical coherence tomography. *PLoS One.* **7** (4), e36135 (2012).
15. Fischer, M. D. *et al.* Noninvasive, in vivo assessment of mouse retinal structure using optical coherence tomography. *PLoS One.* **4** (10), e7507 (2009).
16. Bell, B. A. *et al.* Retinal vasculature of adult zebrafish: in vivo imaging using confocal scanning laser ophthalmoscopy. *Exp Eye Res.* **129** 107-118 (2014).
17. Bailey, T. J., Davis, D. H., Vance, J. E., & Hyde, D. R. Spectral-domain optical coherence tomography as a noninvasive method to assess damaged and regenerating adult zebrafish retinas. *Invest Ophthalmol Vis Sci.* **53** (6), 3126-3138 (2012).
18. Huber, G. *et al.* Spectral domain optical coherence tomography in mouse models of retinal degeneration. *Invest Ophthalmol Vis Sci.* **50** (12), 5888-5895 (2009).

19. Dysli, C., Enzmann, V., Sznitman, R., & Zinkernagel, M. S. Quantitative Analysis of Mouse Retinal Layers Using Automated Segmentation of Spectral Domain Optical Coherence Tomography Images. *Transl Vis Sci Technol.* **4** (4), 9 (2015).
20. Sim, D. A. *et al.* A simple method for in vivo labelling of infiltrating leukocytes in the mouse retina using indocyanine green dye. *Dis Model Mech.* **8** (11), 1479-1487 (2015).
21. Bosco, A., Romero, C. O., Ambati, B. K., & Vetter, M. L. In vivo dynamics of retinal microglial activation during neurodegeneration: confocal ophthalmoscopic imaging and cell morphometry in mouse glaucoma. *J Vis Exp.* (99), e52731 (2015).
22. Acton, J. H., Cubbidge, R. P., King, H., Galsworthy, P., & Gibson, J. M. Drusen detection in retro-mode imaging by a scanning laser ophthalmoscope. *Acta Ophthalmol.* **89** (5), e404-411 (2011).
23. Greenstein, V. C. *et al.* Structural and functional changes associated with normal and abnormal fundus autofluorescence in patients with retinitis pigmentosa. *Retina.* **32** (2), 349-357 (2012).
24. Jung, S. *et al.* Analysis of fractalkine receptor CX(3)CR1 function by targeted deletion and green fluorescent protein reporter gene insertion. *Mol Cell Biol.* **20** (11), 4106-4114 (2000).
25. Wang, X. *et al.* Requirement for Microglia for the Maintenance of Synaptic Function and Integrity in the Mature Retina. *J Neurosci.* **36** (9), 2827-2842 (2016).
26. Ebneter, A., Casson, R. J., Wood, J. P., & Chidlow, G. Microglial activation in the visual pathway in experimental glaucoma: spatiotemporal characterization and correlation with axonal injury. *Invest Ophthalmol Vis Sci.* **51** (12), 6448-6460 (2010).
27. Ebneter, A., Kokona, D., Schneider, N., & Zinkernagel, M. S. Microglia Activation and Recruitment of Circulating Macrophages During Ischemic Experimental Branch Retinal Vein Occlusion. *Invest Ophthalmol Vis Sci.* **58** (2), 944-953 (2017).
28. Lin, Y. L., & Potter-Baker, K. A. Using theoretical models from adult stroke recovery to improve use of non-invasive brain stimulation for children with congenital hemiparesis. *J Neurophysiol.* jn 00258 02017 (2017).
29. Combadiere, C. *et al.* CX3CR1-dependent subretinal microglia cell accumulation is associated with cardinal features of age-related macular degeneration. *J Clin Invest.* **117** (10), 2920-2928 (2007).
30. Bermudez, M. A. *et al.* Time course of cold cataract development in anesthetized mice. *Curr Eye Res.* **36** (3), 278-284 (2011).
31. Toth, C. A. *et al.* A comparison of retinal morphology viewed by optical coherence tomography and by light microscopy. *Arch Ophthalmol.* **115** (11), 1425-1428 (1997).
32. Ebneter, A., Kokona, D., Jovanovic, J., & Zinkernagel, M. S. Dramatic Effect of Oral CSF-1R Kinase Inhibitor on Retinal Microglia Revealed by In Vivo Scanning Laser Ophthalmoscopy. *Transl Vis Sci Technol.* **6** (2), 10 (2017).
33. Gabriele, M. L. *et al.* Reproducibility of spectral-domain optical coherence tomography total retinal thickness measurements in mice. *Invest Ophthalmol Vis Sci.* **51** (12), 6519-6523 (2010).
34. Nakao, S. *et al.* Wide-field laser ophthalmoscopy for mice: a novel evaluation system for retinal/choroidal angiogenesis in mice. *Invest Ophthalmol Vis Sci.* **54** (8), 5288-5293 (2013).
35. Wang, N. K. *et al.* Origin of fundus hyperautofluorescent spots and their role in retinal degeneration in a mouse model of Goldmann-Favre syndrome. *Dis Model Mech.* **6** (5), 1113-1122 (2013).
36. Wang, N. K. *et al.* Cellular origin of fundus autofluorescence in patients and mice with a defective NR2E3 gene. *Br J Ophthalmol.* **93** (9), 1234-1240 (2009).
37. Thanos, S. Sick photoreceptors attract activated microglia from the ganglion cell layer: a model to study the inflammatory cascades in rats with inherited retinal dystrophy. *Brain Res.* **588** (1), 21-28 (1992).
38. Hughes, E. H. *et al.* Generation of activated sialoadhesin-positive microglia during retinal degeneration. *Invest Ophthalmol Vis Sci.* **44** (5), 2229-2234 (2003).

